Clays and Clay Minerals, Vol. 34, No. 2, 187–197, 1986.

MORPHOLOGY OF CLAY MINERALS IN THE SMECTITE-TO-ILLITE CONVERSION SERIES BY SCANNING ELECTRON MICROSCOPY

W. D. KELLER,[1] R. C. REYNOLDS,[2] AND ATSUYUKI INOUE[3]

[1] Department of Geology, University of Missouri–Columbia, Columbia, Missouri 65211
[2] Department of Earth Sciences, Dartmouth College, Hanover, New Hampshire 03755
[3] Geological Institute, College of Arts and Sciences, Chiba University, Chiba 260, Japan

Abstract—The morphology of illite/smectite (I/S) from deeply buried bentonites and hydrothermally altered Tertiary volcanic rocks from Japan changes in parallel with the proportion of expandable layers in the I/S. As viewed by scanning electron microscopy, the morphologies range from the typical "corn-flake," "maple leaf," or "honeycomb" habit of smectite to the typical platy or scalloped (with curled points) habit of illite. Although the changes are more subtle near either end member, at a composition of 60–70% illite layers, the morphology changes from sponge-like or cellular to platy or ribbon-like. The change of morphology at this composition correlates with a change in layer stacking from turbostratic to rotational ordering of the $1M_d$ type. Turbostratic stacking can be thought of as randomly distributed translations of successive layers by any magnitude and in any direction. The rotationally ordered structure, which allows nearly precise juxtaposition of quasihexagonal oxygen surfaces from adjacent layers, probably permits more crystalline regularity in the *a-b* plane, which promotes a more plate-like or sheet-like habit.

Key Words—Burial diagenesis, Hydrothermal alteration, Illite/smectite, Morphology, Scanning electron microscopy, Smectite-to-illite conversion.

INTRODUCTION

Crystal morphologies of clay-mineral families, as observed in scanning electron micrographs (SEM) are characteristically unique and typically are sufficiently different so that morphology and texture can be used as criteria in identifying individual species. For example, bentonite, a volcanogenic montmorillonite-rich mudrock, possesses a distinctly different texture from that of a shale mudrock that is composed of illite or from that of a flint clay, another mudrock composed chiefly of kaolinite. If the smectite of the mudrock is subsequently transformed to illite, as in the smectite-to-illite conversion in a deeply buried shale, it is logical to ask if the change in mineral composition produces a corresponding change in texture and morphology of the rock and its constituent minerals. Moreover, if such a change in morphology does occur, will the textural change that attends the smectite-to-illite conversion during deep burial (Perry and Hower, 1970; Nadeau and Reynolds, 1981) be similar to that caused by the hydrothermal transformation of smectite to illite (Inoue, 1983; Inoue *et al.*, 1978)?

The purpose of the present report is to examine by scanning electron microscopy rocks in which the minerals have been progressively altered or generated from essentially all smectite to essentially all illite, and to illustrate the morphologies of the minerals in various stages of alteration with micrographs. Samples from both environments, i.e., deep burial and hydrothermal alteration, have been examined.

MATERIALS AND METHODS

Materials

The samples used to prepare reference or standard SEMs showing the characteristic morphologies of illite and montmorillonite were chosen from the Source Clays Repository of The Clay Minerals Society, from the original API Reference Clay Minerals, and from other sources as cited in Table 1 and in the captions of the micrographs. For the smectite-to-illite conversion materials, two suites of samples were examined. One suite, representing deep-burial diagenesis of bentonites from the Cretaceous Mancos Shale in the southern Rocky Mountains (designated the MB series), was previously described by Nadeau and Reynolds (1981). It was supplemented by one Ordovician and two Devonian K-bentonites. The Devonian samples were from the Tioga bentonite of middle Devonian (Onondaga) age (Altaner, 1985). The other suite (designated the JHS series), representing the hydrothermal alteration of Tertiary volcanic rock, is from the Shinzan area, Akita Prefecture, northeast Japan, and was described by Inoue and Utada (1983) and Inoue *et al.* (1978). The geology, mineralogy, chemical analyses, and procedures for calculating the I/S ratios of these samples have been covered in detail in the papers cited.

Scanning electron microscopy

The samples were prepared for scanning electron microscopy as follows: Small chips were newly broken from the mineral and rock materials so as to expose

Table 1. Location and properties of illite/smectite samples studied.

Sample	Source[1]	Particle size (μm)	Expandable layers (%)	Reichweite ordering type[2]	Other minerals
WS-4-373	JHS	<2	90	R0 (random)	
WS-4-383	JHS	<2	80	R0	Chlorite
MB-448	Wellington, Utah	<1	65	R0	Kaolinite
WS-2-407	JHS	<2	60	R0	Illite, chlorite
MB-261	Steamboat Springs, Colorado	<1	60	R0	Kaolinite
WS-4-392	JHS	<2	45	R0	Illite
MB-310	Wolcott, Colorado	<1	45	R0	
MB-875	New Castle, Colorado	<1	45	R0–R1	Illite, kaolinite
WS-10-199	JHS	<2	45	R1 (IS)	
MB-892	New Castle, Colorado	<0.5	30	R1	Kaolinite
MB-885	New Castle, Colorado	<0.5	30	R1	
Ordovician K-bentonite	Jefferson County, Missouri	<1	25	>R1 (IS–IIS)	
WS-5-281	JHS	<2	12	R3 (IIIS)	Chlorite
Tioga K-bentonite	Cherry Valley, New York	<0.5	10	R3	Quartz
Tioga K-bentonite	Cove Mountain, Virginia	<1	0		Halloysite/hydrated halloysite, quartz

[1] JHS = Japanese hydrothermal series. These are Tertiary volcanic rocks, Shinzan area, Akita Prefecture, northeast Japan. MB = bentonites from the Mancos Shale, southern Rocky Mountains. The Tioga is a bentonite of middle Devonian (Onondaga) age.

[2] Determined by comparison between observed and calculated X-ray powder diffraction pattern.

clean, fresh fracture surfaces representative of the texture and structure of the rock. The direction of fracture with respect to bedding is not critical in rocks that are essentially isotropic in texture, such as bentonite or flint clay, but the variety of textures in a fissile shale are most clearly seen on a slanted, "stair-step" fracture that exposes both the riser edges and the flat faces of the crystals. Earlier work (Keller, 1946) has shown that the fissility of shales results chiefly from the inherent platy shape and texture of their constituent clastic and diagenetic minerals (usually illite and/or chlorite), rather than from the platiness of these minerals induced mechanically by overburden pressure. A confirmatory example is the refractory clay ("fire clay") described by Keller (1946, 1981) that is chiefly kaolinite, but which is massive in structure beneath a fissile, platy, illitic shale.

To avoid the possibility of introducing artifacts during the sample-preparation procedure, the fractured chips of the clay rocks were not further processed except for sputter-coating the surfaces with a thin film of gold to conduct away excess electric charge from the scanning electron microscope's electron beam. Energy dispersive X-ray spectra (EDX) were obtained when necessary to confirm the identification of materials. Using a JEOL 35 microscope, the clays were examined over a range of magnifications as high as 20,000×, but most textures were best seen in the range 1000 to 13,000×.

X-ray powder diffraction examination

The clay samples studied are described in Table 1, and their X-ray powder diffraction (XRD) patterns are shown in Figures 1–3. Samples were dispersed by ultrasonification, and <2-, <1-, and <0.5-μm particle size fractions were separated by centrifugation. The sized fractions were saturated with Mg^{2+} and prepared for XRD analysis by sucking the suspensions through a 0.45-μm Millipore filter, followed by inverting the filter cakes and transferring them to glass slides, sample-side down. The filter cakes were allowed to dry, after which the filter paper was stripped off. This procedure produced greater preferred orientation than rolling the filter cakes to the point where they adhered to the glass slide. The samples were solvated with ethylene glycol by exposing them to vapor for about 12 hr at 60°C.

XRD patterns were recorded using a Siemens diffractometer equipped with a copper tube and a graphite monochromator. A 1° divergence slit was used in conjunction with the standard D-500 Soller slit array. The oriented clay films were not infinitely thick with respect to CuKα radiation and were shorter (38 mm) than the spread of the incident beam at diffraction angles less than about 10°2θ. Thus, relative intensities were distorted at high (>20°) and low (<10°) values of 2θ. The percentages of illite in the I/S samples were published by Inoue *et al.* (1978) and Inoue and Utada (1983) for the Japanese hydrothermal series. Others were esti-

https://doi.org/10.1346/CCMN.1986.0340209 Published online by Cambridge University Press

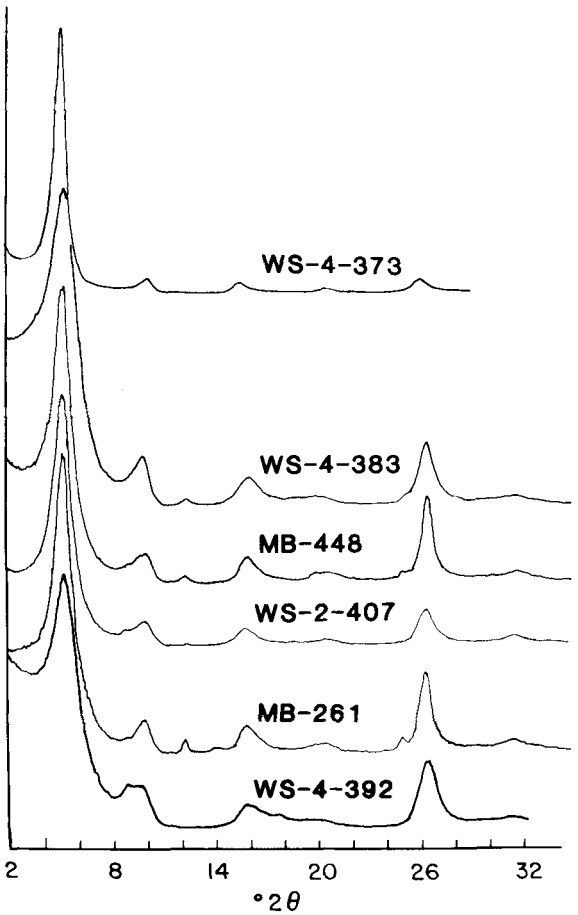

Figure 1. X-ray powder diffraction patterns of oriented, Mg^{2+}-saturated, ethylene glycol-saturated clays; CuKα radiation. For details of analytical conditions, see text. Sources, expandable layer content, particle sizes, ordering types, and other minerals present are listed in Table 1.

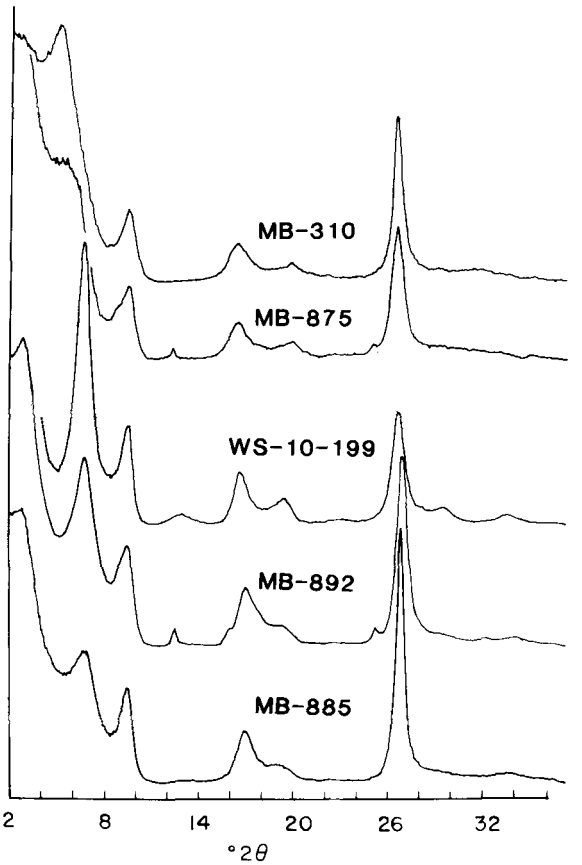

Figure 2. X-ray powder diffraction patterns of oriented, Mg^{2+}-saturated, ethylene glycol-saturated clays; CuKα radiation. For details of analytical conditions, see text. Sources, expandable layer content, particle sizes, ordering types, and other minerals present are listed in Table 1.

mated using the peak positions near 9° and 17°2θ as determined from computer-calculated patterns (Reynolds, 1980) that were modified so that different thicknesses of ethylene glycol could be inserted into the calculations (Środoń, 1980). The ordering type, or Reichweite, was determined by comparisons between observed and calculated diffraction patterns.

Some of the samples contained small amounts of kaolinite (samples MB-448, MB-261, MB-875, and MB-892) or chlorite (samples WS-4-383, WS-2-407, and WS-5-281), and the Tioga K-bentonite from Virginia contained large amounts of what appeared to be interstratified halloysite/hydrated halloysite. The XRD pattern of the Ordovician K-bentonite from Missouri showed a weak shoulder at 3°2θ, and that of sample WS-10-199 had a strong superlattice reflection at 3.1°2θ. The low-angle XRD patterns of these two samples are not shown in Figures 2 and 3 so that a reasonable scale could be maintained for the remaining peaks. For the same reason, the strong reflection near 26.6°2θ for sample WS-5-281 and the Tioga K-bentonite from New York were truncated arbitrarily in Figure 3.

XRD patterns are not reported here for the flint clay, the Silver Hill illite (Hower and Mowatt, 1966), and the Clay Spur and Chambers bentonites because these reference clays are well known and widely available. The Clay Spur and Chambers bentonites were described by Kerr (1951), and Reynolds (1965) published an XRD pattern of the ethylene glycol-solvated form of the Clay Spur material. The XRD pattern of the LaMotte illite is not reported here because our supply of this material became exhausted during the study.

RESULTS AND DISCUSSION

The SEMs shown in this report were selected from numerous micrographs taken at different magnifications and orientations of the samples and are representative of the characteristic morphologies of the samples examined. The magnifications shown are those that best illustrate the distinctive texture of the mineral

https://doi.org/10.1346/CCMN.1986.0340209 Published online by Cambridge University Press

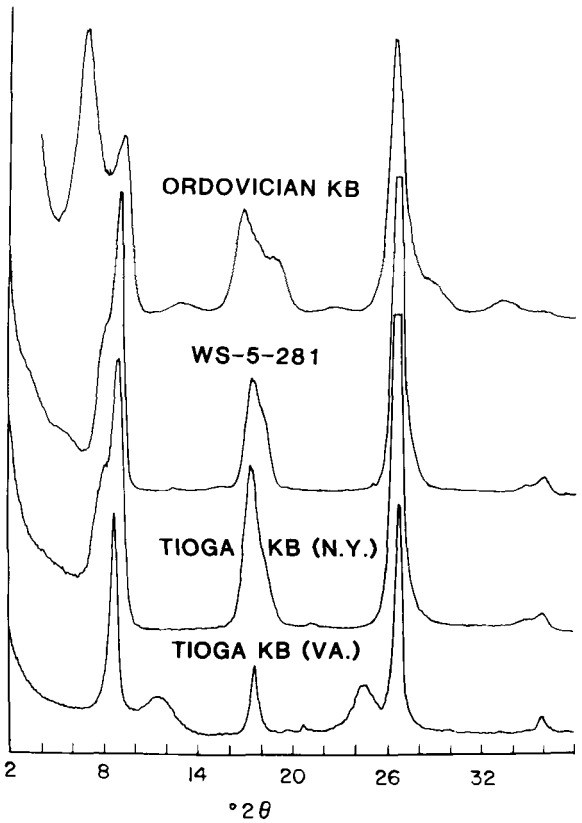

Figure 3. X-ray powder diffraction patterns of oriented, Mg^{2+}-saturated, ethylene glycol-saturated clays; CuKα radiation. For details of analytical conditions, see text. Sources, expandable layer content, particle sizes, ordering types, and other minerals present are listed in Table 1.

or rock. The operating magnification is included in the figure captions to give the microscopist greater insight into the actual experimental conditions.

Morphology of reference clay minerals

Figures 4–6 illustrate the morphologies of reference smectite and illite and provide a basis for comparison with the morphologies of other samples. In Figures 4 and 5, Na-montmorillonite from Clay Spur, Wyoming, and Ca-montmorillonite from Chambers, Arizona, display the "cornflake," "oak leaf," or "cellular" textures that are typical and representative of montmorillonite. Characteristically, the Na-montmorillonite is more open-textured or fluffy than the Ca-montmorillonite, presumably because the Na^+ interlayer ion is more easily hydrated than is Ca^{2+}, and therefore the Na-clay is more easily expanded. That the texture of montmorillonite is developed during its formation from volcanic shards is shown by the partial alteration of shards in the Chambers material (Figure 6). Parallel orientation of parent shards may have produced slight microlineation in the microtexture of the rock, but it is not evident in hand specimens.

Reference illite from the Silver Hill Shale, Montana, is shown in Figure 7 and at higher magnification in Figure 8. These two SEMs illustrate distinctive morphologic features of illite: (1) "ribbon" crystals that, (2) as they coalesce, develop scalloped edges on the coalesced flakes presumably because of non-uniform elongate growth of the ribbons, and (3) confirm by preservation of their ribbed textural pattern the manner by which they grew and coalesced and thereby produced (4) thin, platy crystals that tend to be planar and laminated and which generate fissility in the shale.

A similar ribbon shape is displayed by the authigenic crystals of illite (Figure 9) that grew within a sandstone pore (Cambrian LaMotte Sandstone, southeast Missouri, courtesy of D. Houseknecht). A pattern of ribbons and scalloped edges can also be seen in the Japanese sample WS-5-281 (Figure 10) whose I/S composition was determined to be 88% illite and 12% smectite layers. Thus, illite "ribbons" tend to coalesce to platy, striated crystals which typically are laminar and flat, except that their ends may curl.

The foregoing SEMs demonstrate that crystal morphologies can be used under favorable conditions to distinguish pure smectite from pure illite. Kaolinite, in non-fissile flint clay displays a crystal morphology that is clearly different from those of both illite and smectite (Figure 11). Thus, micromorphologies and textures are physical properties that permissively may be used for mineral identification.

Morphologies of minerals in the smectite-to-illite conversion series

Sample WS-4-373 contains 90% expandable layers (Inoue and Utada, 1983). As seen in Figure 12, the dominant "cornflake" texture is consistent with its high smectite content. Sample WS-4-383 contains 80% expandable layers and shows two slightly different cellular patterns (Figure 13), both of which resemble the morphology of pure smectite. Sample MB-448, a bentonite from the Mancos Shale, contains 65% expandable layers. In Figure 14, the smectite texture is dominant, but closer scrutiny reveals that the edges of some flakes are scalloped and terminate in relatively sharp points that are characteristically displayed by plates of illite (see Figures 7, 8, and 10). Hydrothermal sample WS-2-407 contains 60% expandable layers. In Figure 15, the curvature and flare characteristic of the smectite texture can be seen, but the plates clearly have scalloped edges that terminate in points. The similarity in the development of pointed scallops in these last two clays (i.e., the Mancos bentonite containing 65% expandable layers and the hydrothermal clay containing 60% expandable layers) from radically different petrologic environments, ages, and locations indicates that mineral composition, rather than genetic environment, controlled the morphology of the clay minerals.

Two hydrothermal samples, WS-4-392 and WS-10-

https://doi.org/10.1346/CCMN.1986.0340209 Published online by Cambridge University Press

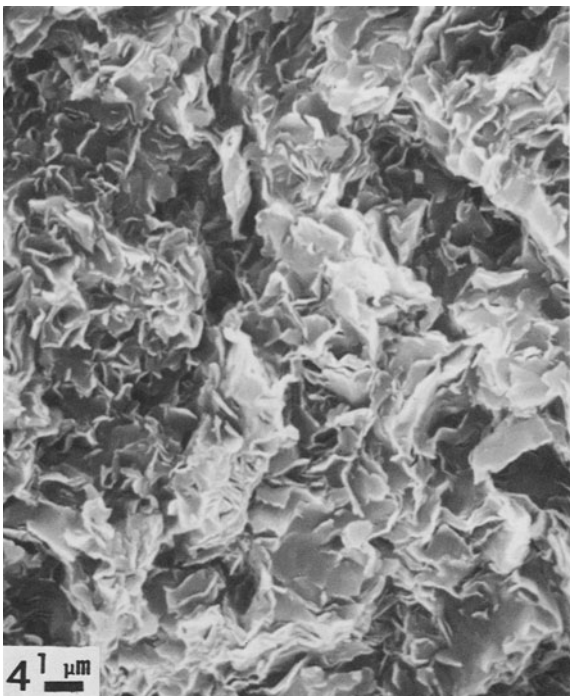

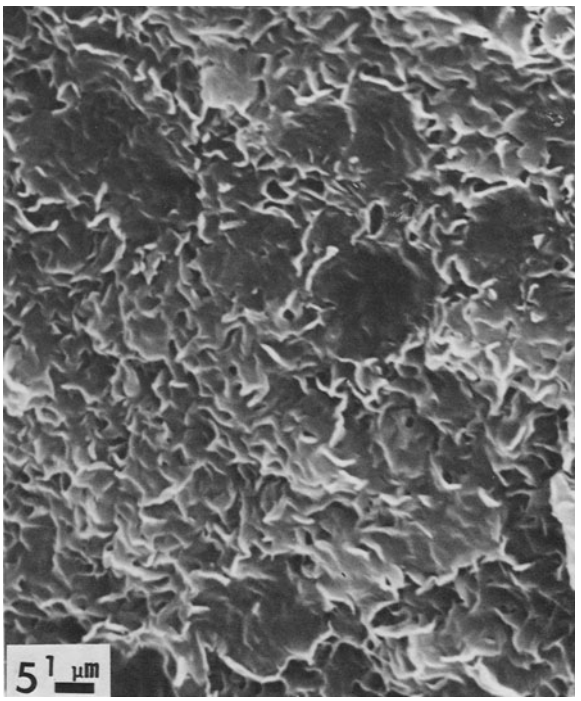

Figure 4. Scanning electron micrograph of sample API-26, Na-montmorillonite from Clay Spur, Wyoming, showing typical expanded, flared, "cornflake" or "oak leaf" texture of Na-montmorillonite; original instrument magnification = 6000×.

Figure 5. Scanning electron micrograph of sample API-23, Ca-montmorillonite, Chambers, Arizona, showing typical, tightly interwoven flakes; original instrument magnification = 6000×.

Figure 6. Scanning electron micrograph of sample API-23, Ca-montmorillonite, Chambers, Arizona, showing almost completely montmorillonized shards; original instrument magnification = 4000×.

Figure 7. Scanning electron micrograph of sample IMt-1, illitic shale, Silver Hill, Montana, showing scalloped, curled edges of relatively large, flat-lying platy crystals of illite; original instrument magnification = 2000×.

https://doi.org/10.1346/CCMN.1986.0340209 Published online by Cambridge University Press

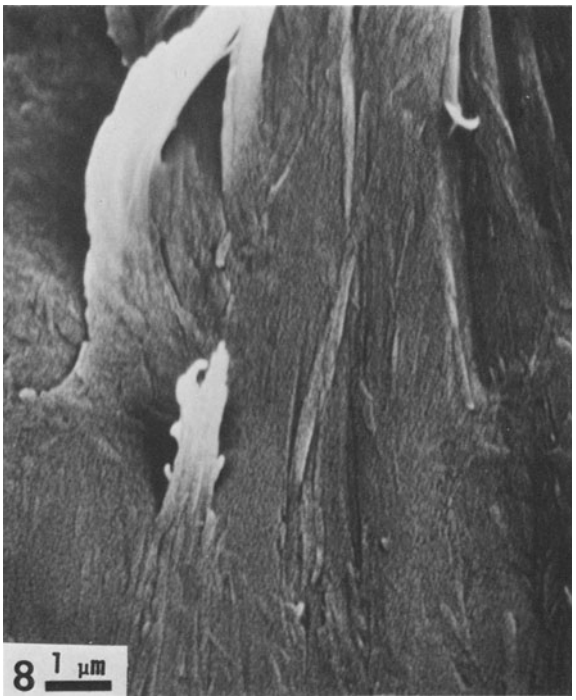

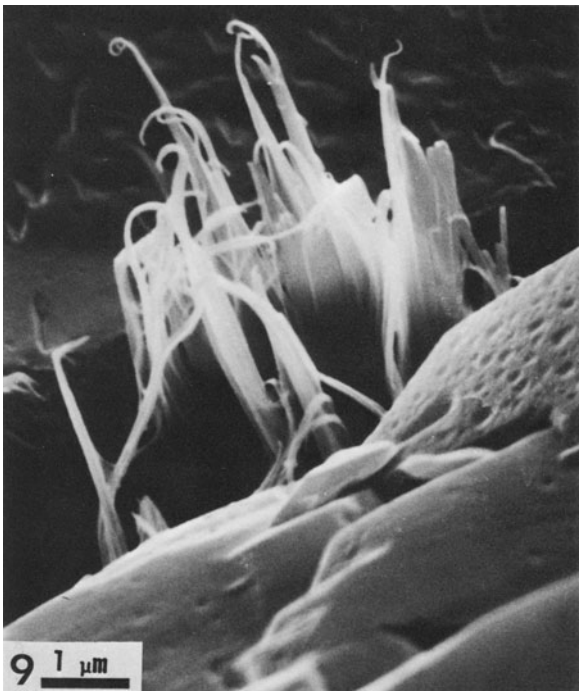

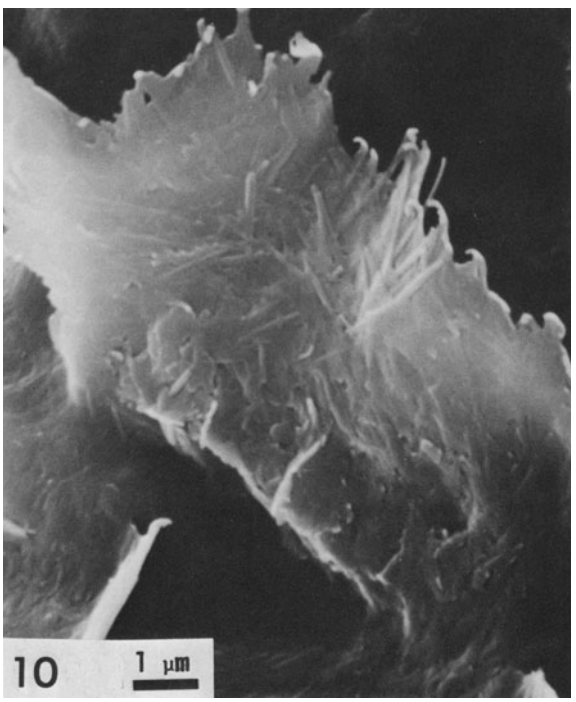

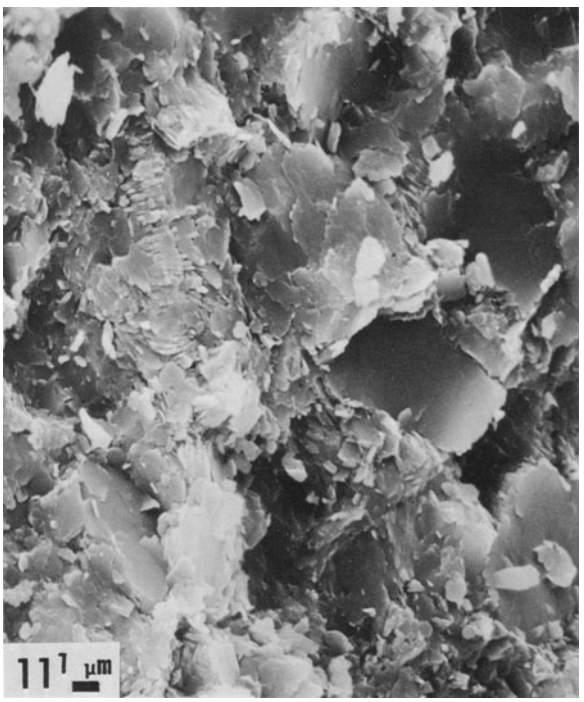

Figure 8. Scanning electron micrograph of enlarged part of Figure 7, showing pattern of platy crystals that formed apparently by coalescence of thin, narrow, "ribbon" crystals of illite; original instrument magnification = 10,000×.

Figure 9. Scanning electron micrograph of "ribbon" crystals of illite crystallized within pore in Cambrian LaMotte sandstone, southeastern Missouri; courtesy of D. Houseknecht; original instrument magnification = 13,000×.

Figure 10. Scanning electron micrograph of sample WS-5-281, Japanese hydrothermal series, showing plate of illite terminating in pointed, scalloped, slightly curled edges. Coalesced "ribbon" crystals of illite end in curved points rising from plate and are apparently less coalesced than others that comprise bulk of plate. Sample contains 12% expandable layers; original instrument magnification = 10,000×.

Figure 11. Scanning electron micrograph of flint clay from Maher deposit, Whitesides, Missouri. Rock is isotextural and consists of randomly oriented, tightly interlocking packets of kaolinite; original instrument magnification = 3600×.

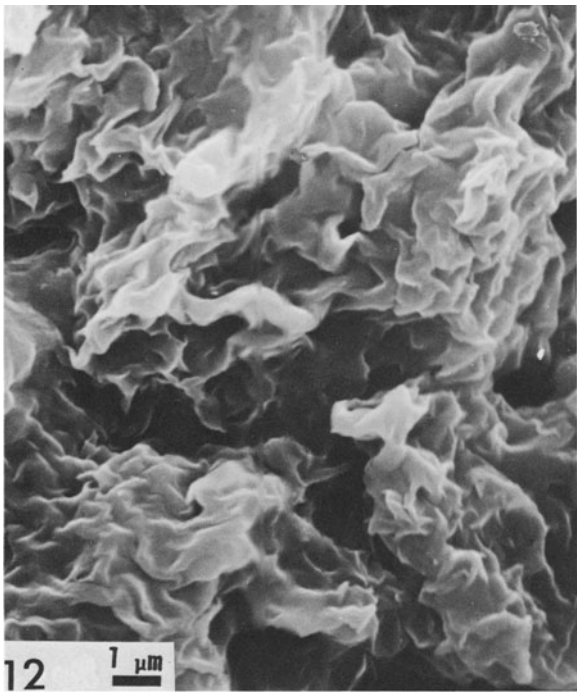

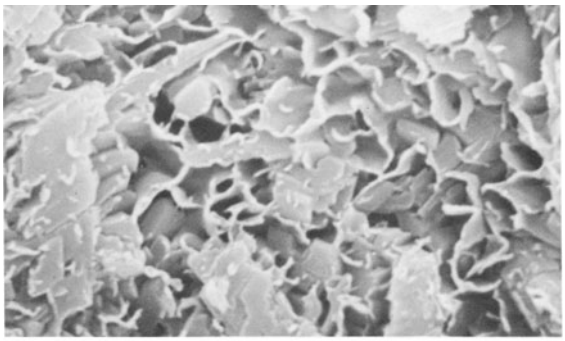

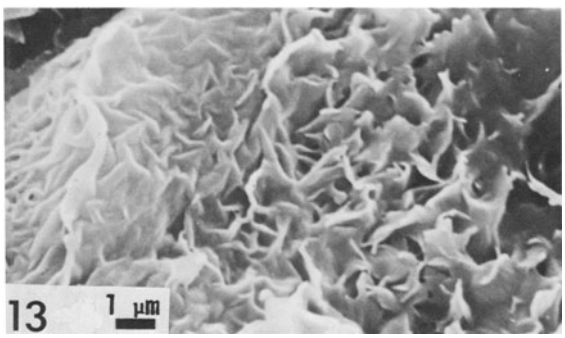

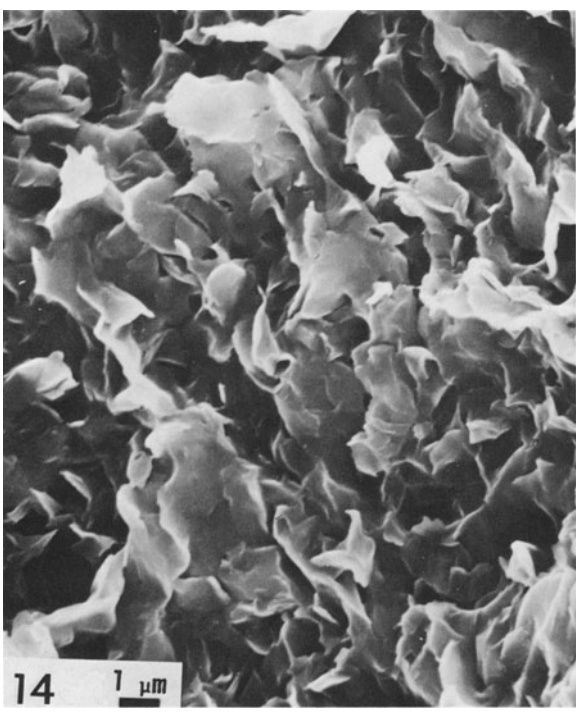

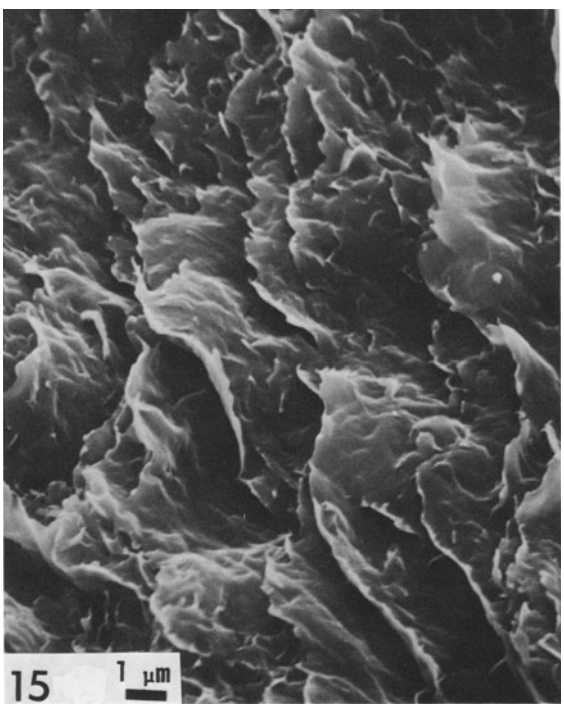

Figure 12. Scanning electron micrograph of sample WS-4-373, Japanese hydrothermal series, containing 90% expandable layers. Texture is similar to that shown in Figure 4; original instrument magnification = 7000×.

Figure 13. Scanning electron micrographs of sample WS-4-383, Japanese hydrothermal series. Sample contains 80% expandable layers and shows crudely cellular, smectitic texture that is less well developed than those shown in Figures 5 and 6; original instrument magnification = 6000×.

Figure 14. Scanning electron micrograph of sample MB-448, bentonite from Mancos Shale. Rock contains 65% expandable layers and shows flared flakes of smectite wherein edges are scalloped into sharp points, some of which are suggestive of illite texture; original instrument magnification = 6000×.

Figure 15. Scanning electron micrograph of sample WS-2-407, Japanese hydrothermal series. Rock contains 60% expandable layers and shows pointed, scalloped edges as in illite as well as curved and flared edges, as in smectite, suggesting a hybrid morphology; original instrument magnification = 6000×.

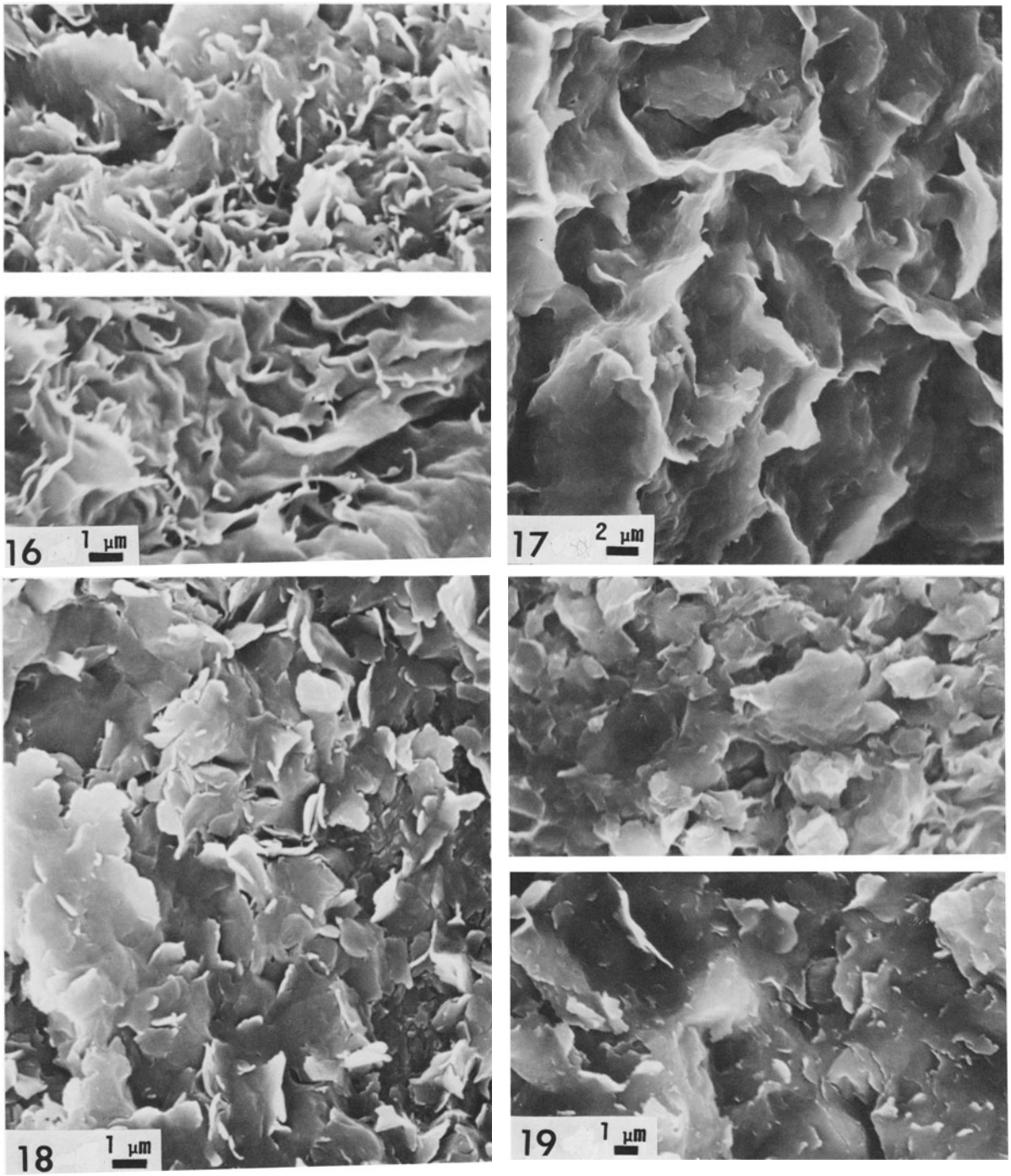

Figure 16. Scanning electron micrographs of samples WS-4-392 (upper) and WS-10-199 (lower), Japanese hydrothermal series. Samples contain about 45% expandable layers and show illite-type scalloped edges and points and some relatively flat-lying plates, suggesting hybrid morphology; original instrument magnification = 6000×.

Figure 17. Scanning electron micrograph of sample MB-875, bentonite from Mancos Shale. Sample contains 45% expandable layers and shows large number of flat-lying flakes whose edges are similar to those of illite and thus transitional between smectite and illite; original instrument magnification = 3000×.

Figure 18. Scanning electron micrograph of sample MB-885, bentonite from Mancos Shale. Sample contains 30% expandable layers and has a morphology closer to that of illite (Figure 10) than to that of smectite (Figures 4 and 5); original instrument magnification = 6000×.

Figure 19. Scanning electron micrographs of bentonite from Mancos Shale (upper) and Ordovician metabentonite from near St. Louis, Missouri (lower). Samples contain about 30% and 25% expandable layers, respectively; original instrument magnification = 4000×.

https://doi.org/10.1346/CCMN.1986.0340209 Published online by Cambridge University Press

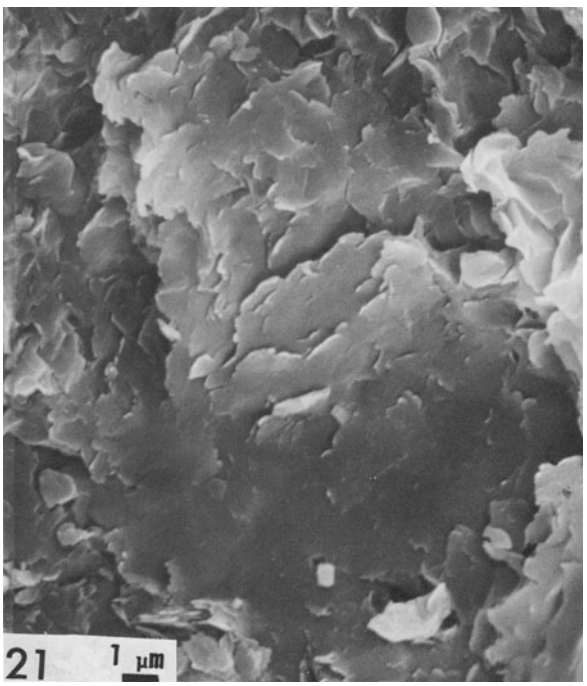

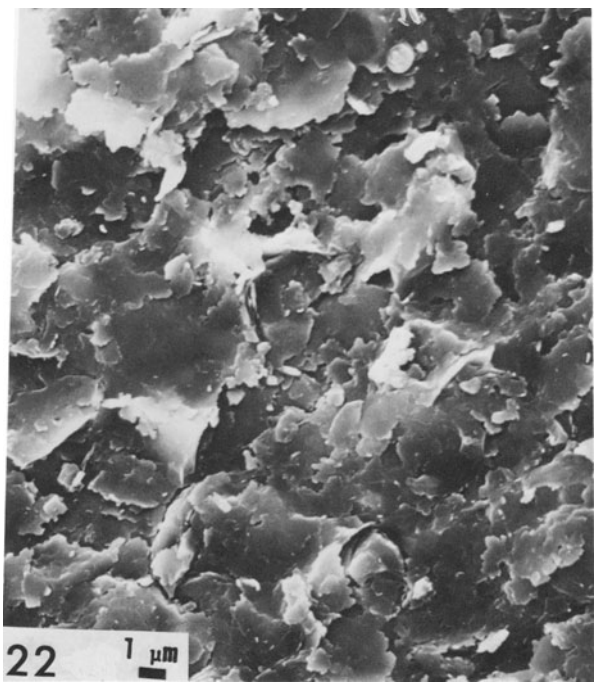

Figure 20. Scanning electron micrograph of sample WS-5-281, Japanese hydrothermal series. Sample contains 12% expandable layers and shows flat, platy texture of illite; original instrument magnification = 1000×. See also scanning electron micrograph of same specimen shown in Figure 10.

Figure 21. Scanning electron micrograph of Tioga K-bentonite, Cherry Valley, New York. Sample contains 10% expandable layers and shows flat-lying plates typical of illite, and dissimilar from texture of smectite; original instrument magnification = 5400×.

Figure 22. Scanning electron micrograph of Tioga K-bentonite, Virginia. Sample is essentially pure illite and shows plates of illite that are scalloped and slightly curled at the edges; original instrument magnification = 4000×.

199, containing 45% expandable layers, are shown in Figure 16. The large amount of relatively sharp points on the crystal flakes indicates substantial illitization. Such changes in morphology are subtle, yet they are real and show a trend that parallels the degree of illitization. Sample MB-875, a bentonite from the Mancos Shale, contains 45% expandable layers. As shown in Figure 17, the flattening of plates is prevalent in contrast to the flaring edges that prevail in pure smectite. Sample MB-885, also from the Mancos Shale, contains 30% expandable layers and appears to be more illitic than smectitic in texture (Figure 18). Here, a difference in the *kind* of pattern, rather than in the degree of modification is apparent. The plates are relatively flat (illitic), except for a curling of the edges, some of which show scallops that locally are pointed.

The most pronounced change in the morphology of smectite-to-illite conversion series samples appears to be at about 45% smectite layers, and the change appears to be essentially complete at about 30% smectite layers. This range of maximum change is the same as that reported by Inoue and Utada (1983) and Perry and Hower (1970) for the development of regular interstratification, whereas, at >45% expandable layers, interstratification was random. We have noted (unpublished data) that with ordering at <45% expandable layers, the turbostratic stacking of smectite gives way to the $n \cdot 60^0$ (Mering, 1975) or $1M_d$ stacking rotations displayed by many illites. Individual unit layers in illite are rotated an exact multiple of 60° with respect to their neighboring layers, thereby producing nearly identical rotational alignment of the two oxygen surfaces on opposite sides of the interlayer space. For illite, such a condition provides potassium with the required 12-fold coordination and allows the necessary contraction along the *c* axis to a value of 10 Å. Apparently, the change in morphology during the smectite-to-illite conversion reflects such polytypic changes in the crystal structure of these minerals.

That the morphology of the minerals in the 25–30% range of expandable layers is dominantly illitic is shown by the texture of sample MB-892 (a bentonite from the Cretaceous Mancos Shale) and the Ordovician K-bentonite from Missouri. These materials unquestionably have illitic textures, and the samples are dominated by a matrix of relatively compact, planar particles from which slightly curled flakes arise. Significantly, the source rocks of these samples are widely separated in location and geologic time. Sample WS-5-281 contains 12% expandable layers. It consists of typical fissile, platy illite particles that are curled on their edges (Figure 20). At higher magnification (Figure 10), platy particles with scalloped pointed edges, supplemented with "ribbons" of illite, are apparent. The Tioga K-bentonites from central New York and Virginia contain 10 and 0% expandable layers, respectively. Texturally, they resemble the reference illites shown in Figures 7 and 8 (see Figures 21 and 22, respectively).

CONCLUSIONS

Crystal morphologies and textures shown by SEMs of clay minerals change progressively in degree or in kind within the smectite-to-illite conversion series. The amount of change, although subtle between small steps in conversion and in the middle range of I/S composition, is clearly diagnostic between end members of the series. Because changes in morphology apparently follow a similar pattern in the smectite-to-illite conversion that results from either deep burial of shale or hydrothermal alteration of volcanic rocks, morphological changes during this process must be influenced chiefly by mineral composition rather than by genetic processes.

The most clearly marked morphological change in the smectite-to-illite conversion series is in the range 45–30% expandable layers, the same range of compositions at which regular or ordered interstratification of I/S becomes significant.

ACKNOWLEDGMENTS

Scanning electron micrography for this paper was supported by NSF Grant EAR 81-19592. We are indebted to an anonymous reviewer, P. C. Franks, and F. A. Mumpton for help in revising the manuscript.

REFERENCES

Altaner, S. A. (1985) Potassium metasomatism and diffusion in Cretaceous K-bentonites from the disturbed belt, northwestern Montana and in the middle Devonian Tioga K-bentonite, eastern U.S.A.: Ph.D. dissertation, University of Illinois, Urbana, Illinois, 193 pp.

Hower, J. and Mowatt, T. C. (1966) The mineralogy of illites and mixed-layer illite/montmorillonites: *Amer. Mineral.* **51,** 825–854.

Inoue, Atsuyuki (1983) Potassium fixation by clay minerals during hydrothermal treatment: *Clays & Clay Minerals* **31,** 81–91.

Inoue, A., Minato, H., and Utada, M. (1978) Mineralogical properties and occurrence of illite/montmorillonite mixed layer minerals from Miocene volcanic glass in Waga-Omono district: *Clay Sci.* **5,** 123–136.

Inoue, A. and Utada, M. (1983) Further investigations of a conversion series of dioctahedral mica/smectites in the Shinzan hydothermal alteration area, northeast Japan: *Clays & Clay Minerals* **31,** 401–412.

Kerr, P. F. (1951) Preliminary reports, reference clay minerals: *American Petroleum Institute Research Project 49.*

Mering, J. (1975) Smectites: in *Soil Components, Vol. 2, Inorganic Compounds,* J. E. Gieseking, ed., Springer-Verlag, New York, 97–119.

Nadeau, P. H. and Reynolds, R. C. (1981) Burial and contact metamorphism in the Mancos Shale: *Clays & Clay Minerals* **29,** 249–259.

Perry, E. A. and Hower, J. (1970) Burial diagenesis in Gulf Coast pelitic sediments: *Clays & Clay Minerals* **18,** 165–177.

Reynolds, R. C. (1965) An X-ray study of an ethylene glycol-montmorillonite complex: *Amer. Mineral.* **50,** 990–1001.

Reynolds, R. C. (1980) Interstratified clay minerals: in *Crystal Structures of Clay Minerals and their X-Ray Identification,* G. W. Brindley and G. Brown, eds., Mineralogical Society, London, 495 pp.

Środoń, J. (1980) Precise identification of illite/smectite interstratifications by X-ray powder diffraction: *Clays & Clay Minerals* **28,** 401–411.

(Received 29 January 1985; accepted 26 October 1985; Ms. 1451)